J Physiol 591.21 (2013) pp 5305–5320

The Journal of Physiology

The emergence of subcellular pacemaker sites for calcium waves and oscillations

Michael Nivala[1], Christopher Y. Ko[1], Melissa Nivala[1], James N. Weiss[1,2] and Zhilin Qu[1]

Departments of [1]Medicine (Cardiology) and [2]Physiology, David Geffen School of Medicine, University of California, Los Angeles, CA 90095, USA

Key points

- Calcium (Ca^{2+}) is fundamental to biological cell function, and Ca^{2+} waves generating oscillatory Ca^{2+} signals are widely observed in many cell types.
- Some experimental studies have shown that Ca^{2+} waves initiate from random locations within the cell, while other studies have shown that waves occur repetitively from preferred locations (pacemaker sites).
- In both ventricular myocyte experiments and computer simulations of a heterogeneous model of coupled Ca^{2+} release units (CRUs), we show that Ca^{2+} waves occur randomly in space and time when the Ca^{2+} level is low, but as the Ca^{2+} level increases, waves occur repetitively from the same sites.
- Ca^{2+} waves are self-organized dynamics of the CRU network, and the wave frequency strongly depends on CRU coupling.
- Using these results, we develop a theory for the entrainment of random oscillators, which provides a unified explanation for the experimental and computational observations.

Abstract Calcium (Ca^{2+}) waves generating oscillatory Ca^{2+} signals are widely observed in biological cells. Experimental studies have shown that under certain conditions, initiation of Ca^{2+} waves is random in space and time, while under other conditions, waves occur repetitively from preferred locations (pacemaker sites) from which they entrain the whole cell. In this study, we use computer simulations to investigate the self-organization of Ca^{2+} sparks into pacemaker sites generating Ca^{2+} oscillations. In both ventricular myocyte experiments and computer simulations of a heterogeneous Ca^{2+} release unit (CRU) network model, we show that Ca^{2+} waves occur randomly in space and time when the Ca^{2+} level is low, but as the Ca^{2+} level increases, waves occur repetitively from the same sites. Our analysis indicates that this transition to entrainment can be attributed to the fact that random Ca^{2+} sparks self-organize into Ca^{2+} oscillations differently at low and high Ca^{2+} levels. At low Ca^{2+}, the whole cell Ca^{2+} oscillation frequency of the coupled CRU system is much slower than that of an isolated single CRU. Compared to a single CRU, the distribution of interspike intervals (ISIs) of the coupled CRU network exhibits a greater variation, and its ISI distribution is asymmetric with respect to the peak, exhibiting a fat tail. At high Ca^{2+}, however, the coupled CRU network has a faster frequency and lesser ISI variation compared to an individual CRU. The ISI distribution of the coupled network no longer exhibits a fat tail and is well-approximated by a Gaussian distribution. This same Ca^{2+} oscillation behaviour can also be achieved by varying the number of ryanodine receptors per CRU or the distance between CRUs. Using these results, we develop a theory for the entrainment of random oscillators which provides a unified explanation for the experimental observations underlying the emergence of pacemaker sites and Ca^{2+} oscillations.

DOI: 10.1113/jphysiol.2013.259960

(Received 6 June 2013; accepted after revision 10 September 2013; first published online 16 September 2013)
Corresponding author Z. Qu: Department of Medicine, David Geffen School of Medicine at UCLA, A2-237 CHS, 650 Charles E. Young Drive South, Los Angeles, CA 90095. Email: zqu@mednet.ucla.edu

Abbreviations Ca^{2+}, calcium; CI, confidence interval; CICR, calcium-induced calcium release; CRU, calcium release unit; DAD, delayed after-depolarization; DS, dyadic space; IP_3, inositol 1,4,5-trisphoshate; ISD, inter-wave initiation site distance; ISI, interspike interval; jSR, junctional sarcoplasmic reticulum; NSR, network sarcoplasmic reticulum; Myo, myoplasm; LCC, L-type calcium channel; RyR, ryanodine receptor; SD, standard deviation; SR, sarcoplasmic reticulum. 2-D, two-dimensional; 3-D, three-dimensional.

Introduction

Calcium (Ca^{2+}) signalling is fundamental to biological function (Berridge *et al.* 2000). In the heart, Ca^{2+} plays crucial roles in pacemaker function underlying the normal heart rhythm (Lakatta *et al.* 2010) and excitation–contraction coupling (Bers, 2002), while dysfunction in intracellular Ca^{2+} signalling can promote heart failure (Anderson *et al.* 2011) and cardiac arrhythmias (ter Keurs & Boyden, 2007). Experimental studies have demonstrated a universal hierarchy of Ca^{2+} signalling dynamics in cardiac myocytes as well as in many other cell types (Marchant *et al.* 1999; Berridge *et al.* 2000; Marchant & Parker, 2001; Cheng & Lederer, 2008; Nivala *et al.* 2012*b*), ranging from Ca^{2+} quarks, sparks, and macrosparks to abortive and finally full waves. This hierarchy can be demonstrated by altering certain parameters, such as extracellular Ca^{2+} concentration (Capogrossi & Lakatta, 1985; Capogrossi *et al.* 1986; Cheng *et al.* 1996) or inositol 1,4,5-trisphoshate (IP_3) concentration (Marchant *et al.* 1999; Marchant & Parker, 2001) in the cell. Specifically, at low Ca^{2+} or IP_3 concentrations, cells predominantly exhibit random single Ca^{2+} sparks with only small fluctuations in the average cytosolic Ca^{2+} of the whole cell. As the Ca^{2+} or IP_3 concentration increases, spark clusters and waves occur, which result in spikes of the whole-cell Ca^{2+} concentration, with randomly irregular interspike intervals (ISIs). As the Ca^{2+} or IP_3 concentration increases further, the Ca^{2+} waves and whole-cell Ca^{2+} spikes become more periodic in time.

Computer modelling studies using stochastic simulations of Ca^{2+} release unit (CRU) networks coupled via Ca^{2+}-induced Ca^{2+} release (CICR; Falcke, 2003; Shuai & Jung, 2003; Izu *et al.* 2006; Skupin *et al.* 2010; Nivala *et al.* 2012*b*) have shown that the initiation of a Ca^{2+} wave is not due to a single spark but requires the formation of a locally self-organized cluster of nearby sparks large enough to propagate non-decrementally by CICR. Recently, we showed that the theory of criticality governs the transition from sparks to waves (Nivala *et al.* 2012*b*), similar to a second-order phase transition in thermodynamic systems (Stanley, 1999). In other words, as the interaction between CRUs via CICR becomes stronger, the spark cluster-size distribution changes from an exponential distribution to a power-law distribution, characteristic of criticality. Long-range correlations, which occur during criticality, facilitate the formation and propagation of Ca^{2+} waves. Theoretically, when the distribution of CRUs is uniform inside a cell, the wave initiation sites should occur randomly and uniformly in space, as demonstrated recently in simulations of a homogeneous CRU network (Nivala *et al.* 2012*b*). This pattern has been observed in many experimental studies (Cheng *et al.* 1996; Wier *et al.* 1997; Marchant & Parker, 2001; Wasserstrom *et al.* 2010). However, in other experimental studies, waves have also been observed to originate repetitively from the same locations in a cell (Rooney *et al.* 1990; Kasai *et al.* 1993; Thorn *et al.* 1993; Simpson *et al.* 1997). The latter is believed to be caused by heterogeneities in the CRU network, such as localized higher concentrations of ryanodine receptors (RyRs) or IP_3 receptors in so-called 'pacemaker' regions of a cell. In our own experiments in ventricular myocytes (data shown in Fig. 3 of our previous publication (Nivala *et al.* 2012*b*) and Fig. 1), we have observed both patterns occurring in the same cell: at Ca^{2+} levels near the spark-to-wave transition, waves occur irregularly and originate randomly from different sites, while at higher Ca^{2+} levels, waves become periodic and tend to originate from preferred locations, acting as pacemaker regions which entrain the whole cell. The question arises, therefore, how can both patterns occur in the same cell? That is, why, at low Ca^{2+} levels, do Ca^{2+} waves arise randomly and irregularly from multiple sites, while at high Ca^{2+} levels, specific pacemaker regions emerge as the predominant source of Ca^{2+} waves generating more periodic Ca^{2+} oscillations? Here we show that this behaviour is a natural consequence of self-organization and random entrainment in a heterogeneous system.

Methods

Cardiac myocyte experiments

The experimental protocol in this study was approved by the UCLA Animal Research Committee and performed in accordance with the NIH *Guide for the Care and Use of Laboratory Animals*.

Ventricular myocyte isolations were performed as previously described (Nivala *et al.* 2012*b*). Briefly, male C57Bl/6 mice of 68 weeks of age were injected intraperitoneally with 800 ml heparin (5000 U/ml) 20–30 min before anesthetization and euthanization with isoflurane (Phoenix Pharmaceuticals). Hearts were quickly excised by thoracotomy and retrogradely perfused on a Langendorff apparatus maintained at 37°C. The enzyme digestion step consisted of perfusing Tyrode's solution containing 1 mg/ml collagenase (Type II, 300 U/mg; Worthington) and 2.8 mg/ml protease (Type XIV, $\geq$ 3.5 U/mg; Sigma) for 13–15 min. Myocytes were dissociated from digested ventricles by gentle mechanical dissociation and used within 46 h. Myocyte membranes were permeabilized for 30–60 s with saponin (0.005% w/v) in nominally Ca^{2+}-free internal solution at room temperature, as previously described in detail (Nivala *et al.* 2012*b*). To facilitate diffusive Ca^{2+}-mediated coupling among CRUs and induce Ca^{2+} signalling events, free Ca^{2+} was incrementally raised in saponin-free internal solution buffered with 0.25 mM EGTA and 0.03 mM Fluo-4 fluorescent Ca^{2+} dye (Invitrogen), using WebMaxC Extended software (maxchelator.stanford.edu) to calculate free $[Ca^{2+}]$. Ca^{2+} imaging was performed using laser confocal microscopy (Zeiss PASCAL 5 system) as described previously (Nivala *et al.* 2012*b*). Fluorescence intensity space–time recordings were acquired in the linescan mode (100 μm line^{-1}, 1.92 ms line^{-1}, 2604 or 5208 lines per recording corresponding to 5 or 10 s long recordings, respectively).

Experimental data analysis

Experimental linescan recordings were analysed using ImageJ software, and statistical analyses were performed using custom Python code (courtesy of Dr. Guillaume Calmettes). The inter-wave initiation site distances (ISDs) and ISIs (see Fig. 1*A*) were measured only from consecutive Ca^{2+} waves that each propagated at least 30 μm. Since the ISD and ISI distributions did not meet conditions for normality, the median was selected as the least biased descriptor for all distributions. Ca^{2+} wave periodicity was described using ISI variance ($\sigma_{|\mathrm{Med}|}$) modified for non-normal distributions and defined as $(\Sigma|\mathrm{ISI} - \mathrm{ISI}_{\mathrm{median}}|)/(N-1)$. In this formula, the median was used in place of the mean as a more appropriate descriptor of non-normal distributions. The absolute value function was used in place of the squaring function, which tends to bias the standard variance towards larger deviations from the mean. Smaller values of $\sigma_{|\mathrm{Med}|}$ reflect greater periodicity. To measure the effect size of intracellular Ca^{2+} levels on ISD and ISI, we used the difference in medians between the low and high Ca^{2+} conditions for each respective interval measure (e.g. median $\mathrm{ISI}_{\mathrm{HighCa}}$ – median $\mathrm{ISI}_{\mathrm{LowCa}}$). To measure the effect size of intracellular Ca^{2+} levels on wave periodicity, we used the difference in $\sigma_{|\mathrm{Med}|}$ between low and high Ca^{2+} conditions (i.e. $\sigma_{|\mathrm{Med}|\mathrm{HighCa}} - \sigma_{|\mathrm{Med}|\mathrm{LowCa}}$). Negative effect sizes indicate smaller value measures at high Ca^{2+} relative to the measures at low Ca^{2+} levels. Confidence intervals (CIs) around observed statistical measures (i.e. median, $\sigma_{|\mathrm{Med}|}$, and effect sizes) were generated using computational bootstrap methods (Efron & Tibshirani, 1991; Manly, 1997; Calmettes *et al.* 2012), which account for smaller and unequal sample sizes and non-normal distributions. Briefly, the statistical measure of interest was calculated from an individual pseudo data sample set generated by randomly resampling, with replacement, values from an actual data sample set (e.g. $\mathrm{ISD}_{\mathrm{HighCa}}$). This process was repeated 100,000 times to generate a distribution of 100,000 estimates of the variability of the statistical measure due to sampling variations. A 99% CI around an observed statistic was determined as the range of values above the 2500th and below the 97,500th value of the distribution of estimates. Statistical significance at the $P < 0.01$ level was established by determining whether effect sizes of zero (i.e. no difference between low and high Ca^{2+} conditions) for a statistical measure fell outside of the 99% CI.

Computational models and methods

The basic computational units are CRUs which are coupled via Ca^{2+} diffusion in myoplasm and sarcoplasmic reticulum (SR) to form a three-dimensional (3-D) cell model (containing 100 × 20 × 10 CRUs). The CRU model was presented in our previous studies (Rovetti *et al.* 2010; Nivala *et al.* 2012*a*,*b*). Briefly, each CRU contains: a junctional SR (jSR) which is diffusively connected to the network SR (NSR), and a dyadic space (DS), which is diffusively connected to the myoplasm (Myo) space. Extracellular Ca^{2+} enters the DS via a leak conductance and the voltage-gated L-type Ca^{2+} channels (LCCs), which were simulated stochastically by a Markov model (Mahajan *et al.* 2008). Ca^{2+} is released from the jSR through its associated cluster of RyRs to the DS. The RyRs were simulated stochastically using a Markov model (Stern *et al.* 1999) in which activation and inactivation of RyRs are regulated by Ca^{2+} in the DS. Each CRU contains 10 LCCs and 100 RyRs. Ca^{2+} is either extruded from the cell via the Na^{+}–Ca^{2+} exchanger or taken back up into the NSR via the SERCA pump. The governing differential equations for the Ca^{2+} concentration in different spaces are:

$$\beta_{\mathrm{m}}(c_{\mathrm{m}})\frac{\partial c_{\mathrm{m}}}{\partial t} = D_{\mathrm{m}}\nabla^2 c_{\mathrm{m}} + J_{\mathrm{m}}, \quad (1)$$

$$\beta_{\mathrm{s}}(c_{\mathrm{s}})\frac{\partial c_{\mathrm{s}}}{\partial t} = D_{\mathrm{s}}\nabla^2 c_{\mathrm{s}} + J_{\mathrm{s}}, \quad (2)$$

$$\beta_{\mathrm{d}}(c_{\mathrm{d}}^{(i)})\frac{\mathrm{d}c_{\mathrm{d}}^{(i)}}{\mathrm{d}t} = J_{\mathrm{d}}^{(i)}, \quad (3)$$

$$\beta_j(c_j^{(i)})\frac{dc_j^{(i)}}{dt} = J_j^{(i)}, \quad (4)$$

where $c_m(x,y,z,t)$ and $c_s(x,y,z,t)$ are the local Ca^{2+} concentrations in the Myo and the NSR, respectively, and $c_d^{(i)}$ and $c_j^{(i)}$ are the Ca^{2+} concentrations in the ith DS and jSR, respectively. β_m, β_s, β_d, and β_j are Ca^{2+} buffering constants, which are instantaneous functions of the Ca^{2+} concentrations in the corresponding spaces, following Wagner & Keizer (1994). J_m, J_s, $J_d^{(i)}$ and $J_j^{(i)}$ are the net Ca^{2+} fluxes for each space. D_m and D_s are the Ca^{2+} diffusion constants in the Myo and the NSR, respectively. To increase the total cellular Ca^{2+} load, we increased the extracellular Ca^{2+} concentration ($[Ca^{2+}]_o$). Note that due to Ca^{2+} spark and wave activity, the SR Ca^{2+} load does not necessarily always increase with $[Ca^{2+}]_o$, but the diastolic cytosolic Ca^{2+} level and total cellular Ca^{2+} load does.

The majority of the simulations in the study were performed in quasi-two-dimensional (2-D) models, in which we coupled the CRUs in 2-D arrays of different sizes. The purposes are twofold: to speed up the simulation for statistics and to allow systematic analyses by comparing behaviours of a single uncoupled CRU with those of coupled CRUs. Since the CRUs in our model are identical, reducing the 3-D model to a quasi-2-D model has relatively small quantitative effects (e.g. shifting the wave threshold to a lower $[Ca^{2+}]_o$ value) while preserving qualitative aspects of the system.

In numerical simulations, the NSR and Myo domains are discretized into 3-D spatial grids using a $0.2 \times 0.2 \times 0.2\ \mu m^3$ spatial resolution. The equations are simulated using an operator splitting method by advancing first the diffusion step and then the flux steps using a first-order forward Euler method with a time step of 0.01 ms. The stochastic transitions of LCCs and RyRs are simulated using the Gillespie's stochastic simulation algorithm (Gillespie, 1977), modified to handle time-dependent rates. All computations are performed on an Intel Xeon 2.53 GHz processor using Graphical Processing Unit (GPU) parallel computing with an NVIDIA Tesla C2050. The details of the computational methods were presented previously (Nivala *et al.* 2012*a*).

Results

Ca^{2+} waves transition from random multiple initiation sites to preferred sites as Ca^{2+} increases in ventricular myocytes

Permeabilized mouse ventricular myocytes were superfused with the fluorescent Ca^{2+} indicator Fluo-4 and imaged with confocal microscopy (see Methods). Figure 1*A* and *B* compare linescans (space–time plots) of the cytoplasmic Ca^{2+} fluorescence at low (100 nM) and high (1000 nM) free Ca^{2+} concentration in the bathing solution. At the low Ca^{2+} concentration, waves were irregular and initiation sites varied randomly, while at the high Ca^{2+} concentration in the same myocyte, waves were more periodic and originated more consistently from the same location. Figure 1*C* shows summary data from multiple cells for the distance between the initiation sites of two consecutive waves, called the inter-wave initiation site distance (ISD). In the case of high Ca^{2+}, more than 80% of the successive wave initiation sites fell in the same 10 μm wide bin, whereas the distribution was much broader for the low Ca^{2+} case. We also calculated the ISI between waves from the same recordings as used for obtaining Fig. 1*C*. The ISI was also much more narrowly distributed in the case of high Ca^{2+} than in the case of low Ca^{2+} (Fig. 1*D*). These differences were statistically significant. For the low Ca^{2+} condition, ISDs ($n = 29$ wave intervals from 22 recordings in 11 cells) exhibited a broad distribution skewed towards larger values ($ISD_{Median} = 14.44\ \mu$m; 99% CI (3.82 μm, 29.96 μm)). For the high Ca^{2+} condition ($n = 171$ wave intervals from 16 recordings in 7 cells), ISDs exhibited a much narrower distribution with less skew and a substantially larger proportion of values ($ISD_{Median} = 2.76\ \mu$m, 99% CI (1.86 μm, 4.82 μm); Fig. 1*C*). The two distributions were statistically significantly different (effect size: $\Delta ISD_{Median} = -11.68\ \mu$m; 99% CI ($-28.06\ \mu$m, $-1.18\ \mu$m); $P < 0.01$). These results indicate multiple sites of wave initiation when Ca^{2+} is low, but smaller excursions mostly limited to a single or few preferred sites when Ca^{2+} is high. Corresponding ISIs (Fig. 1*D*) exhibited a broad distribution ($ISI_{Median} = 3.55$ s; 99% CI (3.23 s, 4.13 s)) under the low Ca^{2+} condition, whereas ISIs exhibited a much narrower distribution and a substantial shift towards smaller values ($ISI_{Median} = 0.47$ s; 99% CI (0.42 s, 0.50 s)) in the high Ca^{2+} condition. The two distributions also were statistically significantly different (effect size: $\Delta ISI_{Median} = -3.08$ s; 99% CI (-3.64 s, -2.79 s)). Thus, Ca^{2+} waves initiate more irregularly at longer intervals when Ca^{2+} is low but become more periodic and frequent when Ca^{2+} is high.

The degree of periodicity was analysed by comparing the average deviation from the median ISI ($\sigma_{|Med|}$, see Methods) at low *versus* high Ca^{2+}. $\sigma_{|Med|}$ decreased from 0.54 s (99% CI (0.34 s, 0.74 s)) at low Ca^{2+} to 0.12 s (99% CI (0.09 s, 0.16 s)) at high Ca^{2+}, which was statistically significant ($P < 0.01$; effect Size: $\Delta\sigma_{|Med|} = -0.41$ s; 99% CI (-0.60 s, -0.21 s)).

Ca^{2+} waves transition from random multiple initiation sites to preferred sites as Ca^{2+} increases in computational models incorporating heterogeneity

Unlike the data in Fig. 1, we found previously that in a simulated homogeneous CRU network, wave initiation

sites were distributed randomly at both low and high Ca^{2+}, even though the ISI decreased and became more periodic at high Ca^{2+} (Nivala *et al.* 2012*b*). However, in a real myocyte, the CRU network contains heterogeneities (Soeller *et al.* 2007; Baddeley *et al.* 2009), both in the size and composition of individual CRUs and in their spatial distribution relative to each other and various intracellular organelles. To test if a simplified heterogeneity in the CRU network could qualitatively account for the experimental observation that Ca^{2+} wave initiation sites become less random as free Ca^{2+} in the bath solution increases (Fig. 1), we introduced a heterogeneous RyR cluster distribution into our 3-D spatially distributed Ca^{2+} cycling model by increasing the number of RyRs per CRU from 100 to 110 in all of the CRUs located in the left 20% of the total cell length (i.e. the $20 \times 20 \times 10$ leftmost CRUs), and observed wave behaviour at various $[Ca^{2+}]_o$. Figures 2*A* and *B* show linescans of free cytoplasmic Ca^{2+} concentration at two different $[Ca^{2+}]_o$ in the myocyte model (see Supplemental Movies for spatiotemporal dynamics). At a low $[Ca^{2+}]_o$, just beyond the transition to full wave behaviour, waves occurred sporadically at random locations. At the higher $[Ca^{2+}]_o$, however, waves became more periodic and originated consistently from

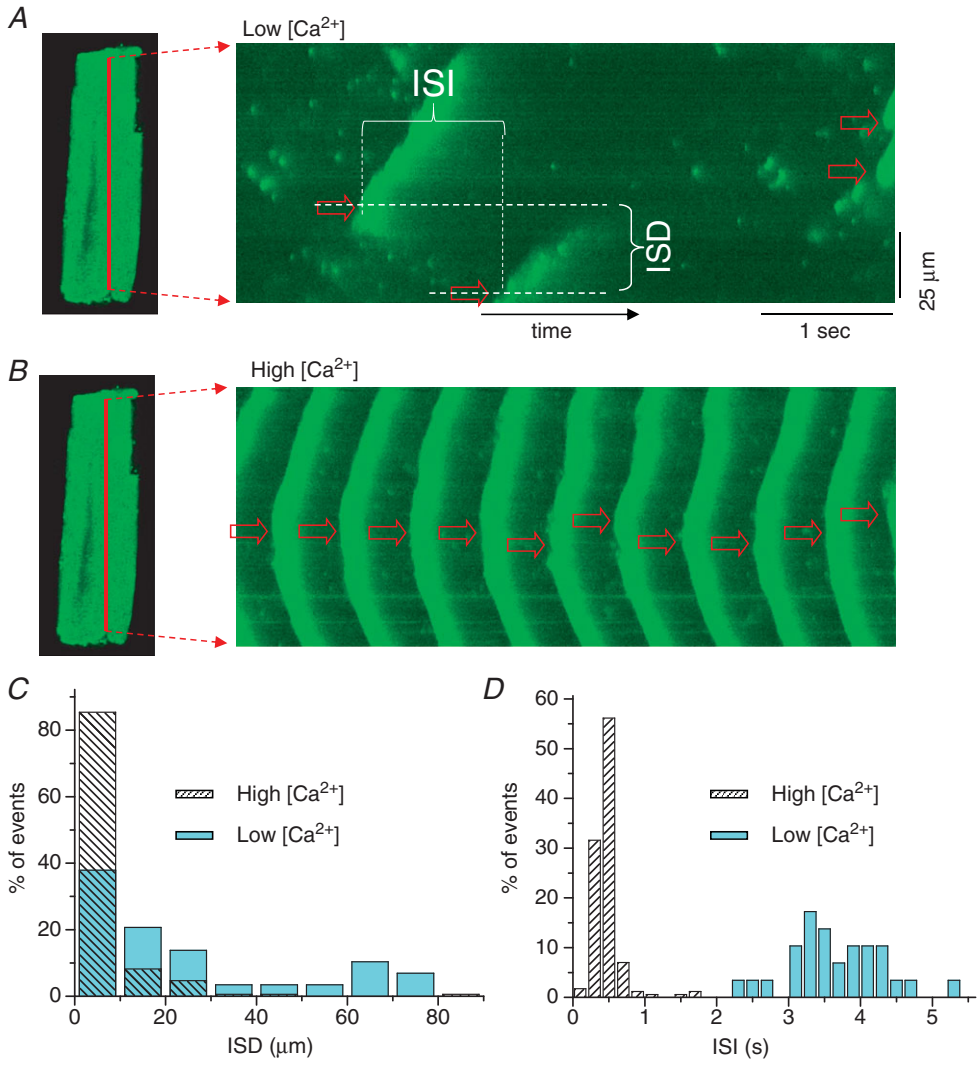

Figure 1. Ca^{2+} wave initiation sites in permeabilized mouse ventricular myocytes
A, a linescan (Fluo-4 fluorescence intensity of a line in the cell *versus* time, as indicated in the left panel) from a myocyte for 100 nM free Ca^{2+} in the solution. The measurements of ISD and ISI are indicated by dashed white lines. *B*, a linescan from the same cell for 1000 nM free Ca^{2+} in the solution. Arrows indicate the wave initiation sites. *C*, summary data for the wave initiation site for low (100 nM) and high (1000 nM) Ca^{2+}. Shown is the distribution of the distance between the initiation sites of two consecutive waves (as illustrated in *A*), called ISD. *D*, summary data for the inter wave interval (i.e. ISI) from the same recordings as in *C*. Due to the limitation of the recording length of the linescan, many long ISIs were missed (an ISI > 2.5 s in a 5 s recording or an ISI > 5 s in a 10 s recording could be missed), indicating that the ISI distribution should be even broader than is shown.

the heterogeneity at the left end of the cell, which acted as a pacemaker site entraining whole-cell oscillations. This agrees with the experimental observations in Fig. 1.

To examine this process in a more systematic fashion and to facilitate the collection of wave initiation statistics, we performed additional analyses using a quasi-2-D version of our spatially distributed Ca^{2+} cycling model, since the full 3-D model was computationally too demanding. The 2-D heterogeneous model consisted of 100 × 20 CRUs, in which the left 20 × 20 CRUs contained 110 RyRs per CRU, and the remaining 80 × 20 CRUs contained 100 RyRs per CRU. Although this heterogeneity was admittedly not physiologically realistic, it served the purpose of creating a large region of the cell with different sensitivity to Ca^{2+}. We then studied how the heterogeneity influenced the wave behaviour over a wide range of $[Ca^{2+}]_o$. Specifically, we measured the extent to which the heterogeneity entrained the whole-cell oscillations by recording the percentage of waves initiated on the left *versus* the right half of the cell for roughly 100 waves, with any deviation from a 50/50 left/right distribution indicating an effect due to heterogeneity. At a low $[Ca^{2+}]_o$ just beyond the transition into the wave regime, the left/right initiation distribution was roughly 60/40, indicating that the heterogeneous region only modestly influenced the wave site generation process (Fig. 2*C*). At increasingly higher $[Ca^{2+}]_o$, the left/right distribution shifted to an increasingly more left dominant pattern, indicating that the degree of entrainment by the identical heterogeneity depends on the Ca^{2+} level of the cell. We also examined the effect of changing the size of the heterogeneity at a fixed $[Ca^{2+}]_o$ (Fig. 2*D*) and observed

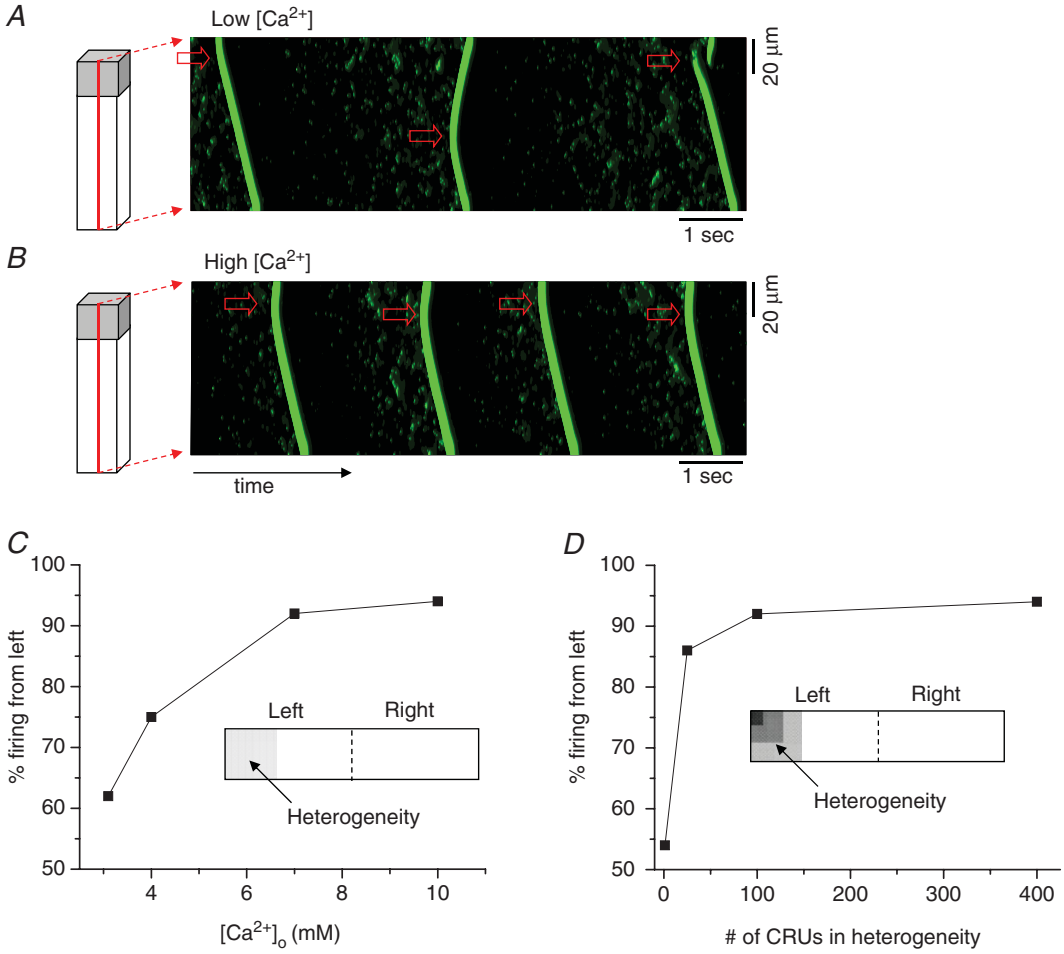

Figure 2. Ca^{2+} wave initiation sites in a 3-D cell model
A, $[Ca^{2+}]_o = 3.1$ mM; *B*, $[Ca^{2+}]_o = 10$ mM. Arrows indicate the wave initiation sites. A heterogeneous region (20 × 20 × 10 CRUs) was included in the left of the network by increasing the number of RyRs from 100 to 110. *C*, percentage of waves that initiated from the left half of the 100 × 20 CRU network model *versus* extracellular Ca^{2+} concentration $[Ca^{2+}]_o$. A heterogeneous region was included in the left 20 × 20 CRUs (see inset) by increasing the number of RyRs from 100 to 110. *D*, percentage of the waves that initiated from the left half of the 100 × 20 CRU network model *versus* the size of the heterogeneous region. The percentages in *C* and *D* are only approximate due to limited run time (roughly 100 total waves).

that for the given conditions, there was a critical size of heterogeneity necessary in order for entrainment to occur. For example, for $[Ca^{2+}]_o = 10$ mM, the entrainment rate increased dramatically to >85% when the size of the heterogeneity reached 5 × 5 CRUs.

Ca^{2+} oscillations as an emergent behaviour of coupled CRUs

To understand how the heterogeneity becomes a progressively more effective pacemaker region entraining Ca^{2+} waves as the Ca^{2+} level increases (Fig. 2), we first studied how Ca^{2+} oscillations emerge in coupled CRU arrays under different conditions. We used the quasi-2-D CRU network model and carried out simulations by varying the sizes of the networks (e.g. 1 × 1 CRU, 2 × 2 CRUs, 3 × 3 CRUs, . . .) to study the spiking properties (e.g. the ISI distribution, its average (<ISI>) and the standard deviation (SD) of the whole system.

Figure 3*A* shows the <ISI> and SD *versus* the number of coupled CRUs for $[Ca^{2+}]_o = 3.1$ mM. For a single isolated CRU, the <ISI> was about 5 s with a SD of 2.5 s. As the number of coupled CRUs increased, both the <ISI> and SD increased. For example, in a 20 × 20 CRU array, the <ISI> was around 20 s with a SD of 13 s. As the number of coupled CRUs increased further, the two quantities saturated at large array sizes. Figure 3*B* shows the averaged whole-system cytosolic Ca^{2+} concentrations ($[Ca^{2+}]_i$) *versus* time for a single uncoupled CRU and a 2-D array of 100 × 20 coupled CRUs. Two important features should be noted. The spark interval in a single uncoupled CRU was much shorter than the Ca^{2+} wave oscillation interval (ISI) in a coupled system. This same phenomenon was demonstrated in recent experiments in cultured human neuroblastoma SH-SY5Y cells by Thurley *et al.* (2011), who showed that the inter-puff intervals were much shorter than the ISIs at the whole-cell level. Another important feature is that the whole system exhibits a much larger random fluctuation than a single unit. This also shows how single channel noise can cause large macroscopic variations at the cellular scale. This random nature of Ca^{2+} oscillations at the whole-cell level has been shown and analysed in studies by Skupin *et al.* (2008) in different cell types and investigated in simulations (Skupin *et al.* 2010).

However, at high $[Ca^{2+}]_o$, the behaviours are different. Figure 3*C* shows the <ISI> and SD for $[Ca^{2+}]_o = 10$ mM. For a single uncoupled CRU, the <ISI> was shorter than at

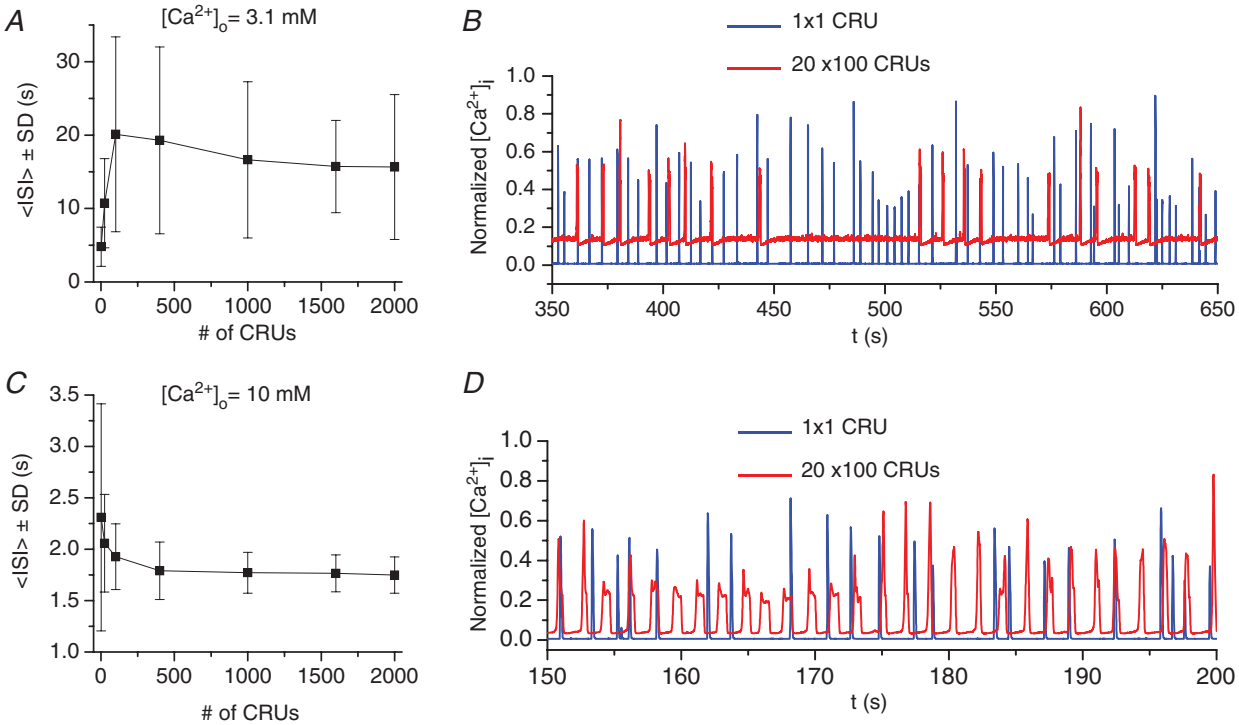

Figure 3. Ca^{2+} excitation dynamics in coupled CRU networks at low Ca^{2+} ($[Ca^{2+}]_o = 3.1$ mM) and high Ca^{2+} ($[Ca^{2+}]_o = 10$ mM)
A, average ISI and standard deviation (<ISI> ± SD) *versus* the number of CRUs, corresponding to 1 × 1, 5 × 5, 10 × 10, 20 × 20, 50 × 20, 80 × 20, 100 × 20 CRUs. *B*, normalized cytosolic Ca^{2+} concentration *versus* time for a single CRU and a 100 × 20 CRU network. *C* and *D*, same as the conditions as *A* and *B* but with $[Ca^{2+}]_o = 10$ mM. Note: many of these distributions are far from Gaussian (see Fig. 7*E*); therefore, <ISI> and SD do not provide a complete description and are only used here to indicate the general trend.

low Ca^{2+}, averaging about 2.3 s with a SD of 1.1 s. Both the <ISI> and SD decreased as the number of CRUs increased and tended to saturate as the system size became large. Figure 3*D* shows the cytosolic Ca^{2+} concentrations *versus* time for a single CRU and an array of 100 × 20 coupled CRUs. Contrary to the low Ca^{2+} case, CRU coupling reduced randomness and accelerated the frequency of the Ca^{2+} wave oscillations. In other words, the Ca^{2+} wave oscillation frequency of the coupled system was faster and more periodic than that of the Ca^{2+} spark frequency of a single uncoupled element. This type of frequency enhancement has also been shown theoretically in coupled random FitzHugh-Nagumo oscillators (Chiang *et al.* 2011) and used to explain the frequency enhancement observed in cultured cardiac monolayers (Chen *et al.* 2009*a*).

Figure 4 summarizes the <ISI> and SD *versus* $[Ca^{2+}]_o$ for a single CRU, an array of 20 × 20 CRUs, and an array of 100 × 20 CRUs, illustrating the transition from frequency suppression to frequency enhancement as $[Ca^{2+}]_o$ increased. As $[Ca^{2+}]_o$ increased from 3.1 mM to 10 mM, the <ISI> of the single CRU decreased from 5 s to about 2.5 s, and the SD from 2.3 s to 1.1 s, almost linearly. In the coupled networks, the <ISI> decreased exponentially from around 20 s to below 2 s, and so did the SD. The network switched from frequency suppression to frequency enhancement at around $[Ca^{2+}]_o = 6$ mM, i.e. for $[Ca^{2+}]_o < 6$ mM, the frequency was lower in the coupled networks than that of a single uncoupled CRU, but for $[Ca^{2+}]_o > 6$ mM, the frequency was higher in the coupled networks.

Besides altering the Ca^{2+} level, this same behaviour was reproduced by changing other parameters. Figure 5 shows results obtained by changing the number of RyRs per CRU. For the low $[Ca^{2+}]_o$, the <ISI> decreased almost linearly from 8 s to 4.5 s in the single uncoupled CRU as the number of RyRs per CRU increased from 20 to 120, accompanied by a similar linear decay in SD (Fig. 5*A*). In an array of 20 × 20 CRUs (Fig. 5*B*), no waves were observed if the number of RyRs per CRU was smaller than 70, and the <ISI> and SD decayed very non-linearly with the RyR number per CRU, from 90 s to 13 s, as the RyR number per CRU increased from 75 to 120. For the high $[Ca^{2+}]_o$, the <ISI> decreased almost linearly from 3 s to 2 s as the RyR number per CRU increased from 20 to 120 (Fig. 5*C*). In an array of 20 × 20 CRUs (Fig. 5*D*), the <ISI> was longer and SD larger than those of the single CRU when the RyR number per CRU was less than 50, but the <ISI> was shorter and SD smaller than those of the single CRU when the RyR number per CRU was greater than 50.

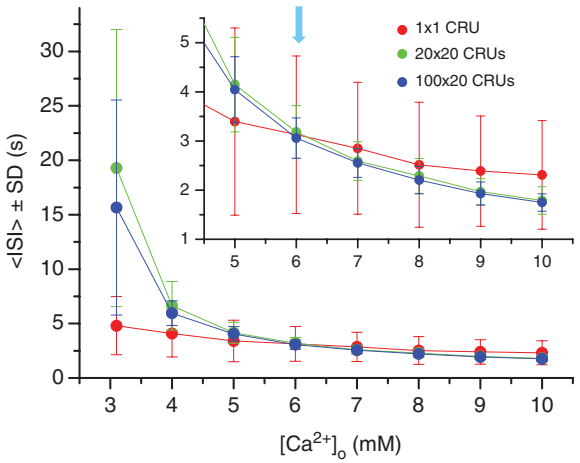

Figure 4. <ISI> ± SD *versus* $[Ca^{2+}]_o$ for a single CRU (red), a 20 × 20 CRU network (green), and a 100 × 20 CRU network (blue)
The inset is a blow-up for <ISI> ± SD from $[Ca^{2+}]_o = 4.5$ to 10 mM. The arrow in the inset indicates the change from frequency suppression to frequency enhancement, at which the <ISI> of a coupled network is shorter than that from a single uncoupled CRU.

We also compared the ISI histograms for both low and high $[Ca^{2+}]_o$ using very long simulations. Panels *A*–*C* of Fig. 6 show the results for high $[Ca^{2+}]_o$. In Fig. 6*A* and *B*, the ISI distribution of a single CRU (Fig. 6*A*) is non-Gaussian, resembled by a gamma distribution, whereas the ISI distribution for a 20 × 20 CRU network (Fig. 6*B*) was well-described by a Gaussian distribution. The range of ISI in the CRU network was much narrower than that for the single CRU. The return map of ISI for the CRU network (Fig. 6*C*) showed no structure, indicating that the consecutive firings were independent. Panels *D*–*F* of Fig. 6 show the results for the low $[Ca^{2+}]_o$. The ISI of the single CRU (Fig. 6*D*) was random and ranged from 0.3 to 14 s. The ISI of the CRU network (Fig. 6*E*), however, peaked at a value 10 times longer than that of the single CRU and had a fat tail. The return map (Fig. 6*F*) again showed no structure. The fat-tailed distribution in the low Ca^{2+} case resulted from runs of firings interspersed with occasional long pauses (see Fig. 3*B*). Note that at both low and high Ca^{2+}, the variation in firing frequency of the single uncoupled CRU did not differ substantially, whereas their variation in the coupled network did. This indicates that these differences in firing properties emerged as a result of coupling between CRUs and dynamical organization, rather than the intrinsic properties of the single CRU *per se*.

Random entrainment in heterogeneous CRU networks

Unlike a system of two deterministic coupled oscillators with resettable phases where the fastest oscillator always entrains the slowest one (Guevara & Glass, 1982; Zeng *et al.* 1991), entrainment in a random system is probabilistic and depends critically on the degree of overlap between the individual ISI distributions. To distinguish the latter case from a deterministic oscillator, classically known as a limit cycle, we adopt the term 'random oscillator.' As shown above, groups of CRUs, which do not limit cycles

themselves, can self-organize into random oscillators, allowing us to recast our heterogeneous CRU network in a simplified manner as a system of two coupled random oscillators by imagining the heterogeneity (e.g. the 20 × 20 CRUs with the higher RyR density) as one random oscillator, and the rest of the CRU network as a second random oscillator. As we show below, the differences between ISI distributions of the two random oscillators at low and high $[Ca^{2+}]_o$ account for the increasing degree of entrainment by the heterogeneity as Ca^{2+} increases.

Consider a system of two coupled random oscillators, and denote one random oscillator by F (for fast) and the other random oscillator by S (for slow), with ISI probability distributions $p_F(x)$ and $p_S(x)$, respectively (Fig. 7*A*). Assume that when one fires, it entrains the other with no delay. Then the probability of S entraining F is:

$$p_{SF} = \int_0^\infty p_F(y) \int_0^y p_S(x)\mathrm{d}x\mathrm{d}y. \qquad (5)$$

Specifically, eqn (5) can be obtained as follows. The probability that F will fire at time y after the previous firing is $p_F(y)$. However, any firing from S earlier than y will entrain site F. Therefore, the conditional probability that a predicted firing of F at time y does not occur is $p_{SF}(y) = p_F(y) \int_0^y p_S(x)\mathrm{d}x$. Summing up all possible firing intervals in site F, one obtains eqn (5). Similarly, the probability of F entraining S is:

$$p_{FS} = \int_0^\infty p_S(y) \int_0^y p_F(x)\mathrm{d}x\mathrm{d}y. \qquad (6)$$

These two equations form the basis of our theory of random entrainment.

One can show that if F and S are Gaussian-distributed with means μ_F and μ_S, and SDs σ_F and σ_S, respectively, then the probability that a random number chosen from distribution F is greater than one chosen from S is also Gaussian-distributed with mean $\mu_F - \mu_S$ and SD $\sqrt{\sigma_F^2 + \sigma_S^2}$, with p_{FS} equal to the area under the curve in the left-half plane. Using this formulation, one can show that F entrains S only as $\mu_F - \mu_S$ surpasses $\sqrt{\sigma_F^2 + \sigma_S^2}$. Figure 8*B* shows the percentage of firing from F *versus*

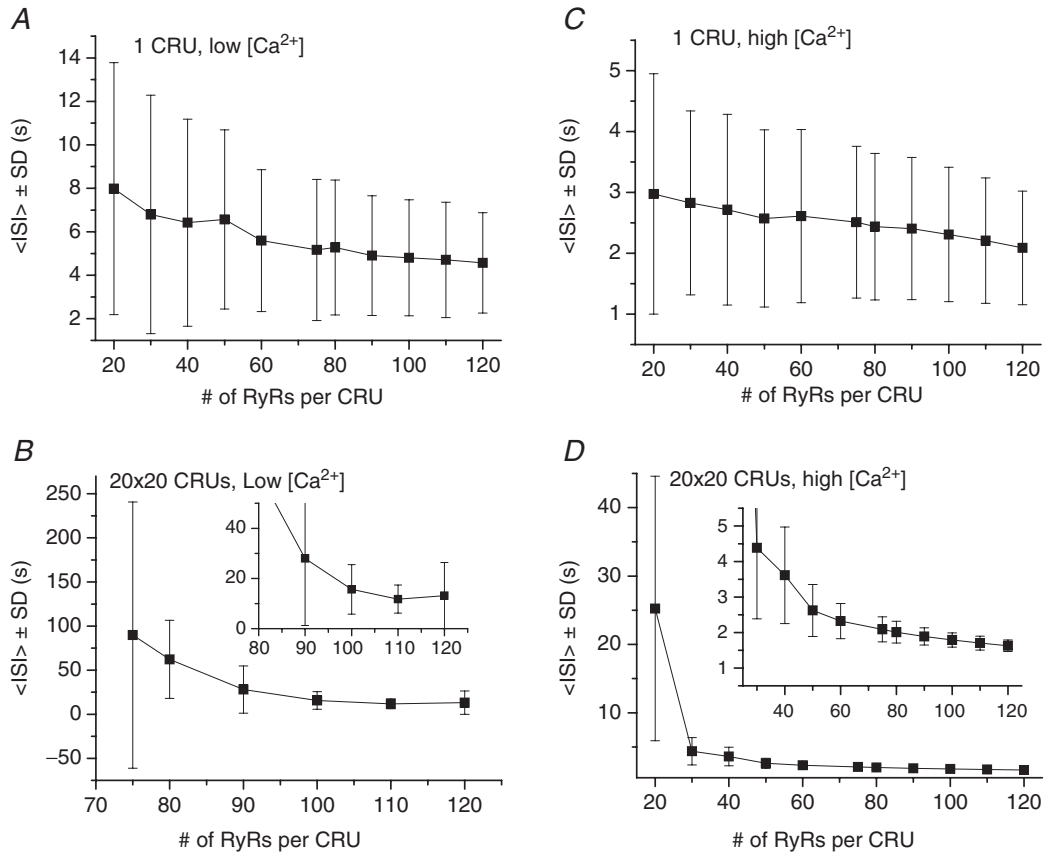

Figure 5. Effects of the number of RyRs per CRU on Ca^{2+} excitation dynamics in a single CRU and a 20 × 20 CRU network
A, <ISI> ± SD *versus* RyR number for a single CRU at low Ca^{2+} ($[Ca^{2+}]_o = 3.1$ mM). *B*, <ISI> ± SD *versus* RyR number for a 20 × 20 CRU at low Ca^{2+} ($[Ca^{2+}]_o = 3.1$ mM). *C*, <ISI> ± SD *versus* RyR number for a single CRU at high Ca^{2+} ($[Ca^{2+}]_o = 10$ mM). *D*, <ISI> ± SD *versus* RyR number for a 20 × 20 CRU at high Ca^{2+} ($[Ca^{2+}]_o = 10$ mM). The insets in *C* and *D* are blow-ups for large RyR numbers.

the shift Δ ($= \mu_F - \mu_S$) for different SDs (σ), showing that the entrainment increases with Δ and decreases with σ. The results are intuitive, i.e. for larger Δ or smaller σ, the two distributions overlap less, and thus the fast one can better entrain the slow one. This simple result may be sufficient to explain the observations in experiments and in our simulations that Ca^{2+} waves tended to originate from roughly the same location at high Ca^{2+} but occurred randomly in space and time at low Ca^{2+}. That is, the SD at low Ca^{2+} is much larger than that at high Ca^{2+}. Even though the difference in firing frequency is also larger, the very large SD at low Ca^{2+} causes the fast region to fail to entrain the slow region.

In addition to the broadness of the distribution, the fat tail of the ISI distribution at low Ca^{2+} levels may also contribute to the reduction of entrainment. The long ISIs in the fat tail allow short firings to occur from the slow site and entrain the fast site, reducing the efficacy of the fast site entraining the slow site. To study this effect, we truncated the Gaussian distribution at the right side and added a fat tail (in the form $C(x - x_0)^{-1}$). Figure 7*C* shows the percentage of firing from the fast site *versus* the joint point (x_c) of the combined distributions, showing that adding the tail reduces the entrainment. We also performed computer simulations using the ISI data for the computer simulation of a CRU network shown in Fig. 6*E*, showing that cutting the fat tail enhances entrainment (Fig. 7*D*).

Discussion

The transition from Ca^{2+} sparks to Ca^{2+} waves and oscillations has been the subject of many experimental (Cheng *et al.* 1996; Parker *et al.* 1996; Bootman *et al.* 1997; Wier *et al.* 1997; Callamaras *et al.* 1998; Marchant *et al.* 1999; Marchant & Parker, 2001) and simulation (Falcke, 2003; Izu *et al.* 2006; Skupin & Falcke, 2009; Skupin *et al.* 2010; Nivala *et al.* 2012*b*) studies. In our previous study (Nivala *et al.* 2012*b*), we showed that, in the transition from sparks to waves, spark clusters self-organize due to CICR. This process exhibits a power-law distribution, which is a hallmark of criticality,

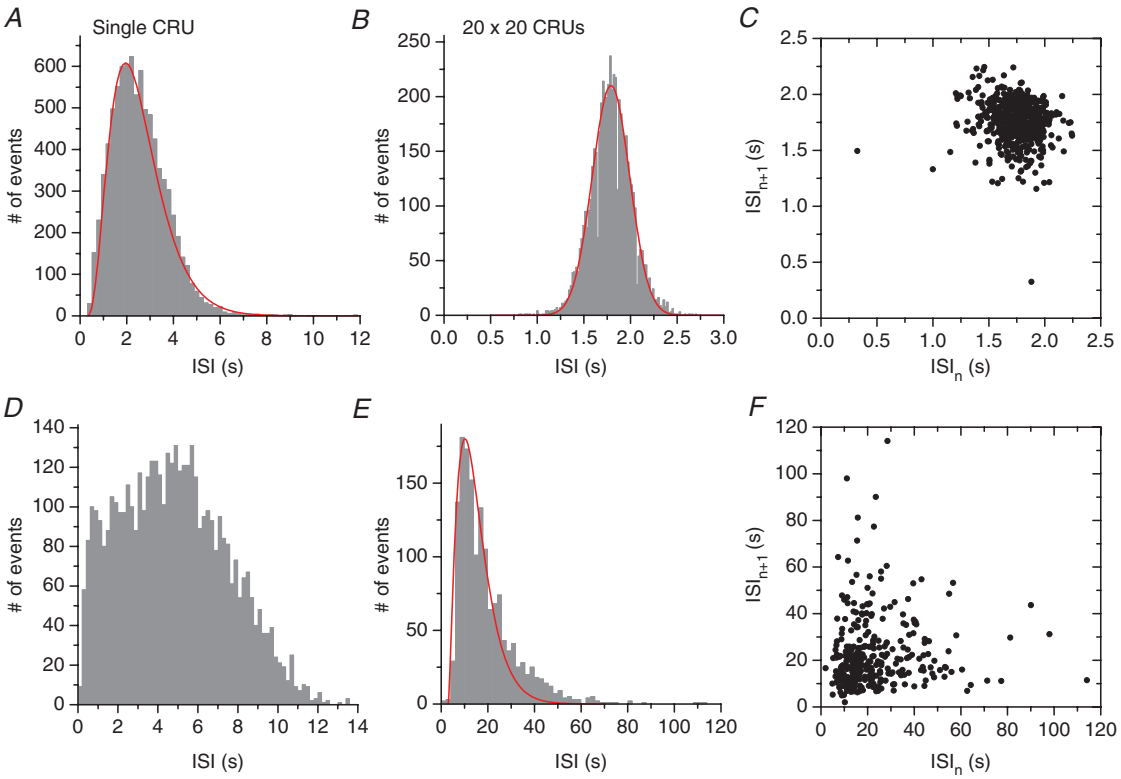

Figure 6. ISI histograms and return maps for low and high Ca^{2+}
A, ISI histogram for high Ca^{2+} ($[Ca^{2+}]_o = 10$ mM) for a single CRU. The red curve is a reference distribution which is a gamma distribution function: $h(x) = 0.0000135(x - 0.3)^{2.75}e^{-(x-0.3)/0.8}$ for $x > 0.3$ s. *B*, ISI histogram for high Ca^{2+} ($[Ca^{2+}]_o = 10$ mM) for a 20 × 20 CRU network. The red curve is a Gaussian distribution function: $h(x) = 210e^{-\frac{1}{2}\left(\frac{x-1.79}{0.2}\right)^2}$ (x is in units of seconds). *C*, return map plotting ISI_{n+1} *versus* ISI_n for the high Ca^{2+} case in *B*. *D*, ISI histogram for low Ca^{2+} ($[Ca^{2+}]_o = 3.1$ mM) for a single CRU. *E*, ISI histogram for low Ca^{2+} ($[Ca^{2+}]_o = 3.1$ mM) for a 20 × 20 CRU network. Red curve is a gamma distribution function: $h(x) = 0.00132(x - 3)^{1.5}e^{-(x-3)/4.8}$ for $x > 3$ s. The fat tail cannot be captured by the gamma function. *F*, return map plotting ISI_{n+1} *versus* ISI_n for the low Ca^{2+} case in *E*.

a dynamical phenomenon widely studied in statistical physics (Stanley, 1999) and in many natural systems (Bak, 1997). In this study, we used computer simulation to further study the dynamics underlying the transition from sparks to waves and global cell-wide oscillations by comparing the Ca^{2+} release dynamics in a single CRU to that in coupled CRU networks with or without subcellular heterogeneities. Our simulation results and theoretical analyses provide mechanistic insights into a variety of experimental observations relating to the origin of Ca^{2+} waves underlying Ca^{2+} oscillations and pacemaking by Ca^{2+} clocks in biological cells.

Dynamical organization in spark-to-wave transitions and oscillations

A Ca^{2+} spark may cause a neighbouring CRU to fire via Ca^{2+} diffusion and CICR, which may then cause its neighbours to fire, and so on. If this chain process is persistent, a Ca^{2+} wave forms and propagates. This is commonly observed in experiments and is considered as the mechanism by which Ca^{2+} sparks initiate Ca^{2+} waves (Cheng *et al.* 1996; Wier *et al.* 1997; Keizer & Smith, 1998; Keizer *et al.* 1998). However, the persistence of the chain of spark-induced sparks may not be sustainable due to the random latency of CRU firing and the recovery of neighbouring CRUs from spontaneous firings. In fact, the vast majority of sparks in a cell do not initiate Ca^{2+} waves (Cheng *et al.* 1996; Wier *et al.* 1997). Our previous study (Nivala *et al.* 2012*b*) showed that the spark-to-wave transition is similar to a second-order phase transition in statistical physics. At very low Ca^{2+} levels, Ca^{2+} sparks occur randomly and sparsely, and thus, no macroscopic Ca^{2+} events occur. As Ca^{2+} increases, Ca^{2+} sparks form clusters with the cluster size distribution exhibiting a power-law, inducing large fluctuations in the local Ca^{2+} concentration, which eventually trigger macroscopic Ca^{2+} waves. As Ca^{2+} increases further, CRUs fire in a more synchronous manner, and the global Ca^{2+} signal becomes more periodic. This provides a formal theoretical basis for the spark-to-wave transitions and long-range correlations observed in intracellular Ca^{2+} signalling.

In this study, our computer simulations show that the spiking behaviour of groups of CRUs cannot be decomposed into the individual dynamics of the CRUs themselves. When the interaction between CRUs is weak (e.g. at low Ca^{2+} levels or low RyR or IP_3 receptor density), the frequency of global firing in a CRU network is much slower than that of a single CRU. This indicates that the organization process for wave initiation dominates over the time dynamics of single CRU firings (sparks), implying that a dynamic time scale for sparks to self-organize into global events has emerged from the CRU network. In other words, the time scale to form a cluster of sufficient size to initiate a Ca^{2+} wave is very long compared to the sparking rate of individual CRUs, so that a CRU is more likely to be activated as a primary spark and only occasionally as a secondary spark triggered by a Ca^{2+} wave. This directly

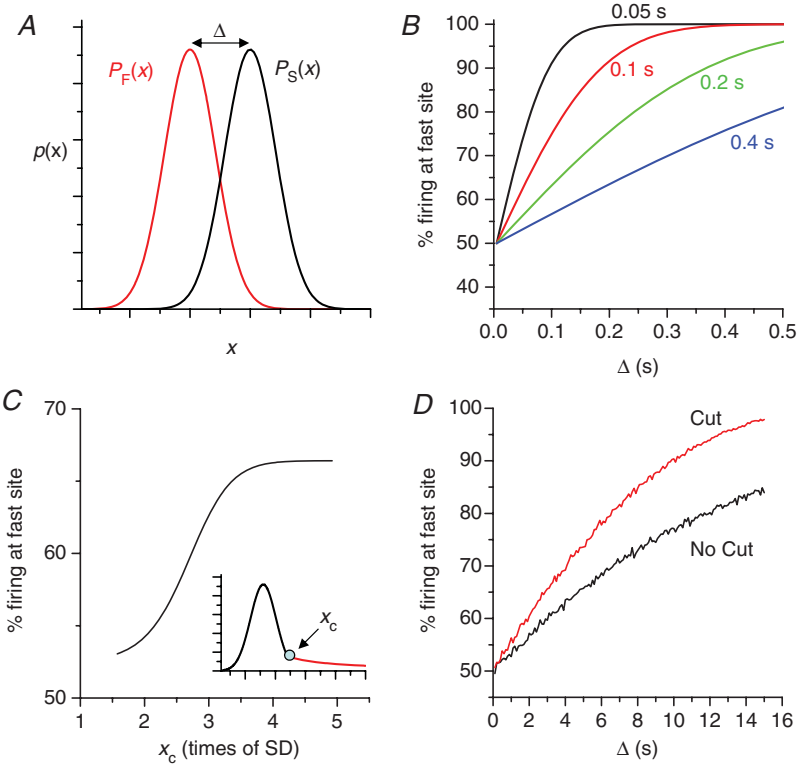

Figure 7. Theoretical analyses for random entrainment
A, illustration of the distribution setup used in *B*. *B*, percentage of firing originating from the fast site *versus* Δ for different standard deviations (labelled) for Gaussian distribution: $p(x) = \frac{1}{\sigma\sqrt{2\pi}} e^{-\frac{1}{2}(\frac{x-\mu}{\sigma})^2}$ (x is in units of seconds), obtained using eqns 5 and 6. $\mu_F = 2$ s. *C*, percentage of firing originating from the fast site *versus* x_c (as indicated in the inset) for asymmetric distribution. $\Delta = 1.5$ s. The Gaussian distribution function is: $h(x) = C_1 e^{-\frac{1}{2}(\frac{x-8.2}{2.5})^2}$ and the fat tail is: $h(x) = C_2(x - x_0)^{-1}$ (x is in units of seconds). *D*, percentage of firing originating from the fast site *versus* the shift Δ from simulations using data from the histogram in Fig. 6*E*. Specifically, we assume that the two firing sites have the same ISI histogram as in Fig. 6*E*, one with a shift of Δ. In the case of fat-tail cutting (red curve), the ISIs greater than 25 s were dropped.

agrees with the experimental observations in cultured human neuroblastoma SH-SY5Y cells by Thurley *et al.* (2011)). As shown by our statistics (Fig. 6*E*), this dynamic time scale exhibits a fat-tailed distribution, a hallmark of self-organization and criticality.

At high Ca^{2+} levels, on the other hand, the global firing frequency is faster than the individual firing frequency of a single uncoupled CRU. Since at high Ca^{2+}, RyRs are more sensitive, a firing CRU has a high probability of recruiting its neighbours to fire, accelerating the global firing frequency. In this case, the dynamic time scale is limited by RyR recovery time and SR refilling time. In other words, the time scale to form a cluster of sufficient size to initiate a Ca^{2+} wave becomes shorter than the sparking rate of an isolated uncoupled CRU, such that most CRUs are activated as secondary sparks by the Ca^{2+} wave before they fire spontaneously as primary sparks. This acceleration of firing in coupled CRU networks at high $[Ca^{2+}]_o$ is similar to the frequency enhancement shown in coupled random FitzHugh-Nagumo oscillators (Chiang *et al.* 2011) in which the frequency of the coupled oscillators is faster than the uncoupled ones. Note that altering $[Ca^{2+}]_o$ or RyR density alters the firing frequency of the single CRU, mostly in a linear manner, but the effect on the global firing frequency is much larger and non-linear, indicating that the interaction (or coupling) between the CRUs plays an important role. The coupling effect can be directly demonstrated in computer simulations by changing the distance between CRUs, i.e. the closer the CRUs, the stronger the coupling. Figure 8*A* shows an ISI histogram from a 20 × 20 CRU network for low Ca^{2+} ($[Ca^{2+}]_o = 3.1$ mM), in which the CRU spacing was changed from 1 μm to 0.8 μm. The <ISI> became much shorter (from ∼20 s to ∼8 s), and the SD much smaller (from ∼13 s to ∼1 s). The distribution lost its fat tail and resembled a Gaussian distribution. The effect of CRU spacing on Ca^{2+} wave formation was studied previously in computer simulations by Izu *et al.* (2006)), with similar results.

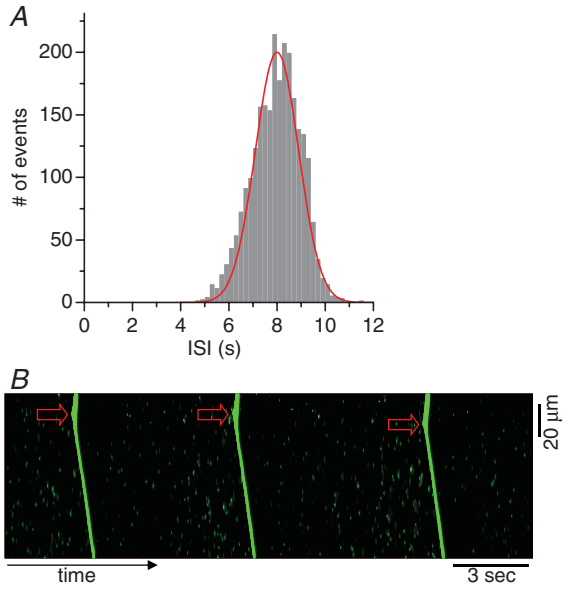

Figure 8. Effects of decreased CRU spacing on ISI and entrainment at low Ca^{2+} ($[Ca^{2+}]_o = 3.1$ mM)
A, ISI histogram from a 20 × 20 CRU network with CRU spacing 0.8 μm. The red curve is a Gaussian distribution function: $h(x) = 200e^{-\frac{1}{2}(\frac{x-8}{0.9})^2}$ (x is in units of seconds). *B*, Ca^{2+} wave initiation sites in a 100 × 20 CRU network cell model. Arrows indicate the wave initiation sites. A heterogeneous region (25 × 25 CRUs) with CRU spacing decreased from 1.0 μm to 0.8 μm was included in the left of the network.

Roles of subcellular heterogeneities

In uniform models such as the CRU network simulated in our previous study (Nivala *et al.* 2012*b*), Ca^{2+} waves organized randomly in space. However, real cells are not uniform and heterogeneities exist, for example, in the number of RyRs (or IP_3 receptors) per CRU, distances between neighbouring CRUs, and discontinuities caused by other intracellular organelles and membrane invaginations (Soeller *et al.* 2007; Baddeley *et al.* 2009). In heterogeneous deterministically excitable systems, the fastest firing site (even if it is only slightly faster than the others) always entrains the whole system, unless conduction breaks occur between firing sites (Xie *et al.* 2001*b*; Qu & Weiss, 2005). In heterogeneous randomly excitable systems, however, the randomness of the firings allows entrainment to be intermittent. As shown in our theoretical analysis, the rate of entrainment depends not only on the difference in firing rates, but also on the broadness and the shape of the ISI distribution. In our simulations, the ISI distribution is much narrower at high Ca^{2+} than at low Ca^{2+}, making entrainment much more efficient at high Ca^{2+}, explaining our experimental observations. Furthermore, the fat-tailed ISI morphology that results from a system being near criticality significantly contributes to the failure of entrainment at low Ca^{2+}.

In heterogeneous excitable systems, the spatial scale of heterogeneity plays an important role for the wave behaviours (Xie *et al.* 2001*a*). As shown in Fig. 2*D*, the entrainment depends on the size of the heterogeneity. In fact, if we increase the number of RyRs from 100 to 110 in 20% of CRUs whose spatial location is chosen randomly from a uniform distribution, then entrainment is lost, and wave dynamics are similar to a homogeneous system. We also used a Gaussian distribution of RyR cluster size (with an average 100 RyRs and standard deviation 10) in our simulation and failed to observe the formation of stable pacemaker sites at high Ca^{2+}. Instead, we still observed pacemaker sites occurring randomly in space as in the homogeneous system. Therefore, the spatial

scale or correlation of RyR cluster size heterogeneity is important for the formation of stable pacemaker sites. Since, to our knowledge, the spatial correlation of RyR cluster size in cardiac myocytes has yet to be characterized experimentally, we chose to use a very simple yet extreme form of heterogeneity to study the effects of heterogeneities in CRU networks in the present study. Even though our heterogeneous CRU network model is not physiologically realistic, this extreme case is useful because it demonstrates that even with such an extreme heterogeneity, the effects of the heterogeneity are minimal at low Ca^{2+} and are only unmasked at high Ca^{2+}. We believe that the general mechanisms of random entrainment will still hold in more realistic heterogeneous systems. In addition, real cells most likely contain multiple heterogeneities, and our theory of random entrainment is easily generalized to more than two coupled random oscillators. In such cases, the degree to which each pacemaker region entrains cellular oscillations depends on the relative overlap of multiple ISI distributions, and multiple pacemaker sites can co-exist.

It should be noted that the scenario in which entrainment occurs at high Ca^{2+} but fails at low Ca^{2+} is only relative. If the system is highly heterogeneous such that the heterogeneous region has a much narrower distribution and faster frequency than other regions, entrainment can still occur at low Ca^{2+}. This is demonstrated in a simulation shown in Fig. 8, in which we made the CRU spacing shorter (from CRU spacing 1 μm to 0.8 μm) at low Ca^{2+} and found that almost all firings originated from the heterogeneous region. In this case, entrainment occurs because the ISI is shorter and much less variable than for control CRU spacing.

It is also important to note that individual CRUs in a heterogeneous region do not oscillate periodically as limit cycles when uncoupled. Periodic pacemaking is still a self-organized phenomenon of a group of randomly firing CRUs. As shown in our simulations, when the coupled CRU network exhibits a strong periodicity, the frequency is faster and much less variable than a single CRU. Thus, the periodicity of the pacemaker site depends strongly and directly on the coupling between CRUs.

Implications for Ca^{2+} cycling dynamics in the heart

Intracellular Ca^{2+} cycling in cardiac systems is not only required for excitation–contraction coupling but also plays important roles in generating both the normal heart rhythm under physiological conditions (Lakatta *et al.* 2010) and life-threatening arrhythmias under pathophysiological conditions of Ca^{2+} overload (ter Keurs & Boyden, 2007). Results from this and our previous study (Nivala *et al.* 2012*b*) may provide new mechanistic insights into these dynamics.

For example, heart rate variability during sinus rhythm has been shown to exhibit power-law (fractal) behaviours (Kobayashi & Musha, 1982; Ivanov *et al.* 1996). This feature is often attributed to autonomic tone, but cardiac preparations which lack autonomic innervation, such as cultured neonatal cardiac monolayers (Kucera *et al.* 2000; Ponard *et al.* 2007), also exhibited a power-law distribution of beating intervals. Although simulations suggested that a Poisson distribution of ion channel protein turnover fluctuations could give rise to power-law behaviour of heart rate variability in this setting, our findings may provide an alternative mechanism related to Ca^{2+} cycling, which is now recognized, together with voltage-dependent oscillations, to play a fundamental role in sino-atrial nodal pacemaking (Vinogradova & Lakatta, 2009; Vinogradova *et al.* 2010). Prior to the action potential upstroke, the occurrence of local Ca^{2+} releases increases inward Na^+–Ca^{2+} exchanger current to facilitate diastolic depolarization. The local Ca^{2+} releases occur more or less randomly in space and time, and their periods, which vary from beat to beat, correlate linearly with the cycle lengths of sino-atrial nodal cell oscillations. The local Ca^{2+} releases are not random single sparks but rather self-organized spark clusters, as also demonstrated in a recent modelling study (Maltsev *et al.* 2011). It is intriguing to speculate that during the transition from Ca^{2+} sparks to whole-cell oscillations, the power-law spark clustering and fat-tailed ISI distribution occur via criticality, potentially contributing to the power-law behaviour in heart rate variability. This is a promising area for future sino-atrial nodal cell and cell network modelling.

Under pathophysiological conditions in atrial and ventricular myocytes and in Purkinje cells, Ca^{2+} waves activate Ca^{2+}-sensitive inward currents such as Na^+–Ca^{2+} exchanger to cause delayed after-depolarizations (DADs), which are arrhythmogenic (ter Keurs & Boyden, 2007). In multicellular tissue, however, a Ca^{2+} wave from a single myocyte cannot generate enough inward current to cause a DAD since its resting voltage is clamped by the neighbouring myocytes without Ca^{2+} waves (Fujiwara *et al.* 2008). To overcome this source–sink mismatch, Ca^{2+} waves have to occur synchronously in tens to thousands for a DAD to occur (Xie *et al.* 2010). Our results may help to explain how this happens, since as Ca^{2+} increases, the <ISI> and SD of Ca^{2+} waves both decrease markedly (Fig. 2). In coupled myocytes with similar Ca^{2+} cycling properties, this would naturally lead to a synchronization of the timing of Ca^{2+} waves in neighbouring myocytes as the Ca^{2+} load increased, as observed in multicellular tissue when Ca^{2+} loading has been varied by rapid pacing (Fujiwara *et al.* 2008; Wasserstrom *et al.* 2010). In failing hearts or genetic models of catecholaminergic polymorphic ventricular tachycardia, RyRs are more sensitive to Ca^{2+} and thus leakier. Even though SR Ca^{2+} load is lower, the increase in RyR sensitivity may enhance CRU coupling, which facilitates Ca^{2+} wave formation and DADs. Moreover, in failing myocytes, the CRU spacing

becomes shorter (Chen-Izu *et al.* 2007) and facilitates wave formation. Heterogeneity may also be enhanced in failing myocytes due to T-tubule disruption and disorganization to promote Ca^{2+} waves.

An important question is what determines the timing of the occurrence of Ca^{2+} waves in cardiac myocytes. Sobie *et al.* (2006) and Ramay *et al.* (2011) showed that the time constant of recovery of Ca^{2+} spark amplitude is ∼100 ms, and the intervals between consecutive sparks are on the order of a couple of hundred milliseconds. The recovery time constant is determined by SR refilling and RyR sensitivity. Brochet *et al.* (2005) have shown that the local SR refilling time is less than 100 ms. Therefore, if the occurrence of Ca^{2+} waves was determined by the refractory period and SR refilling time, Ca^{2+} waves should occur at intervals on the order of a couple of hundred milliseconds. However, Ca^{2+} waves occur at intervals of seconds or even longer, which are much longer than the SR refilling time and the recovery time of the CRU, indicating that the occurrence of Ca^{2+} waves is not solely determined by CRU refractoriness and SR refilling. In a recent experimental study, Belevych *et al.* (2012) demonstrated that Ca^{2+} waves occur in a certain time period, which they call the 'idle period,' after the RyRs are recovered from inactivation and the SR is refilled. Our study shows that Ca^{2+} waves are emergent properties of the CRU network, which depends not only on the properties of the individual CRUs, but also strongly on the coupling between CRUs. The idle period identified by Belevych *et al.* is thus the time for sparks to self-organize into waves, i.e. the idle period is the self-organization period for a critical size of spark clusters to form and initiate a wave.

Limitations

The Ca^{2+} cycling model in this study was developed based on the ventricular myocyte and may be too specific to extrapolate the details of Ca^{2+} cycling dynamics in other types of cells in which the CRUs consist of IP_3 receptor clusters (Falcke, 2003; Shuai & Jung, 2003). Conversely, the detailed subcellular structure of ventricular myocytes and regulation of CRUs are much more complex than the simple heterogeneities modelled in this study (Soeller & Cannell, 1999; Soeller *et al.* 2007; Baddeley *et al.* 2009; Hake *et al.* 2012). The CRUs are identical in our models, but in real cells, even in ventricular myocytes, they are not. For example, CRUs close to the cell surface exhibit different sarcolemma ion channels than those deep inside the cell. These may cause additional interesting dynamics. In addition, different RyR models (Jafri *et al.* 1998; Stern *et al.* 1999; Sobie *et al.* 2002; Restrepo *et al.* 2008; Chen *et al.* 2009*b*) may give rise to different whole-cell Ca^{2+} cycling dynamics, which need to be further investigated in modelling studies.

The computational simulations were done using a model of a myocyte with an intact sarcolemma in which Ca^{2+} content in the cell was changed by altering $[Ca^{2+}]_o$. Experimentally, however, it is difficult to control the Ca^{2+} level in an intact cell by changing $[Ca^{2+}]_o$. Therefore, the experiments were performed on permeabilized cells, allowing intracellular Ca^{2+} to be directly controlled, after verifying that similar results were obtained in the model when the sarcolemma was removed to simulate a permeabilized cell. We feel justified in this approach since it was not the purpose of the present study to obtain strict quantitative agreement between the experiments and the modelling but rather to develop a general dynamical theory for pacemaker generation in cardiac myocytes.

Despite these limitations, our present study provides novel mechanistic insights into how the microscopic random events of intracellular Ca^{2+} cycling (Ca^{2+} sparks) integrate into global events like Ca^{2+} waves and oscillations in cardiac myocytes and in other cell types, as well as general insights into the collective dynamics of coupled random excitable elements.

References

Anderson ME, Brown JH & Bers DM (2011). CaMKII in myocardial hypertrophy and heart failure. *J Mol Cell Cardiol* **51**, 468–473.

Baddeley D, Jayasinghe ID, Lam L, Rossberger S, Cannell MB & Soeller C (2009). Optical single-channel resolution imaging of the ryanodine receptor distribution in rat cardiac myocytes. *Proc Natl Acad Sci U S A* **106**, 22275–22280.

Bak P (1997). *How Nature Works: The Science of Self-Organized Criticality*. Oxford University Press, New York.

Belevych AE, Terentyev D, Terentyeva R, Ho HT, Gyorke I, Bonilla IM, Carnes CA, Billman GE & Gyorke S (2012). Shortened Ca^{2+} signalling refractoriness underlies cellular arrhythmogenesis in a postinfarction model of sudden cardiac death. *Circ Res* **110**, 569–577.

Berridge MJ, Lipp P & Bootman MD (2000). The versatility and universality of calcium signalling. *Nat Rev Mol Cell Biol* **1**, 11–21.

Bers DM (2002). Cardiac excitation–contraction coupling. *Nature* **415**, 198–205.

Bootman MD, Berridge MJ & Lipp P (1997). Cooking with calcium: the recipes for composing global signals from elementary events. *Cell* **91**, 367–373.

Brochet DX, Yang D, Di Maio A, Lederer WJ, Franzini-Armstrong C & Cheng H (2005). Ca^{2+} blinks: rapid nanoscopic store calcium signalling. *Proc Natl Acad Sci U S A* **102**, 3099–3104.

Callamaras N, Marchant JS, Sun XP & Parker I (1998). Activation and co-ordination of $InsP_3$-mediated elementary Ca^{2+} events during global Ca^{2+} signals in *Xenopus* oocytes. *J Physiol* **509**, 81–91.

Calmettes G, Drummond GB & Vowler SL (2012). Making do with what we have: use your bootstraps. *J Physiol* **590**, 3403–3406.

Capogrossi MC, Kort AA, Spurgeon HA & Lakatta EG (1986). Single adult rabbit and rat cardiac myocytes retain the Ca^{2+}- and species-dependent systolic and diastolic contractile properties of intact muscle. *J Gen Physiol* **88**, 589–613.

Capogrossi MC & Lakatta EG (1985). Frequency modulation and synchronization of spontaneous oscillations in cardiac cells. *Am J Physiol Heart Circ Physiol* **248**, H412–H418.

Chen W, Cheng SC, Avalos E, Drugova O, Osipov G, Lai P-Y & Chan CK (2009*a*). Synchronization in growing heterogeneous media. *EPL (Europhysics Letters)* **86**, 18001.

Chen W, Wasserstrom JA & Shiferaw Y (2009*b*). Role of coupled gating between cardiac ryanodine receptors in the genesis of triggered arrhythmias. *Am J Physiol Heart Circ Physiol* **297**, H171–H180.

Cheng H, Lederer MR, Lederer WJ & Cannell MB (1996). Calcium sparks and $[Ca^{2+}]$i waves in cardiac myocytes. *Am J Physiol Cell Physiol* **270**, C148–C159.

Cheng H & Lederer WJ (2008). Calcium sparks. *Physiol Rev* **88**, 1491–1545.

Chen-Izu Y, Ward CW, Stark W Jr, Banyasz T, Sumandea MP, Balke CW, Izu LT & Wehrens XH (2007). Phosphorylation of RyR2 and shortening of RyR2 cluster spacing in spontaneously hypertensive rat with heart failure. *Am J Physiol Heart Circ Physiol* **293**, H2409–H2417.

Chiang WY, Lai PY & Chan CK (2011). Frequency enhancement in coupled noisy excitable elements. *Phys Rev Lett* **106**, 254102.

Efron B & Tibshirani R (1991). Statistical data analysis in the computer age. *Science* **253**, 390–395.

Falcke M (2003). On the role of stochastic channel behaviour in intracellular Ca^{2+} dynamics. *Biophys J* **84**, 42–56.

Fujiwara K, Tanaka H, Mani H, Nakagami T & Takamatsu T (2008). Burst emergence of intracellular Ca^{2+} waves evokes arrhythmogenic oscillatory depolarization via the Na^{+}–Ca^{2+} exchanger: simultaneous confocal recording of membrane potential and intracellular Ca^{2+} in the heart. *Circ Res* **103**, 509–518.

Gillespie DT (1977). Exact stochastic simulation of coupled chemical reactions. *J Phys Chem* **81**, 2340–2361.

Guevara MR & Glass L (1982). Phase locking, period doubling bifurcations and chaos in a mathematical model of a periodically driven oscillator: a theory for the entrainment of biological oscillators and the generation of cardiac dysrhythmias. *J Math Biol* **14**, 1–23.

Hake J, Edwards AG, Yu Z, Kekenes-Huskey PM, Michailova AP, McCammon JA, Holst MJ, Hoshijima M & McCulloch AD (2012). Modeling cardiac calcium sparks in a three-dimensional reconstruction of a calcium release unit. *J Physiol* **590**, 4403–4422.

Ivanov PC, Rosenblum MG, Peng CK, Mietus J, Havlin S, Stanley HE and Goldberger AL (1996). Scaling behaviour of heartbeat intervals obtained by wavelet-based time series analysis. *Nature* **383**, 323–327.

Izu LT, Means SA, Shadid JN, Chen-Izu Y & Balke CW (2006). Interplay of ryanodine receptor distribution and calcium dynamics. *Biophys J* **91**, 95–112.

Jafri MS, Rice JJ & Winslow RL (1998). Cardiac Ca^{2+} dynamics: the roles of ryanodine receptor adaptation and sarcoplasmic reticulum load. *Biophys J* **74**, 1149–1168.

Kasai H, Li YX & Miyashita Y (1993). Subcellular distribution of Ca^{2+} release channels underlying Ca^{2+} waves and oscillations in exocrine pancreas. *Cell* **74**, 669–677.

Keizer J & Smith GD (1998). Spark-to-wave transition: saltatory transmission of calcium waves in cardiac myocytes. *Biophys Chem* **72**, 87–100.

Keizer J, Smith GD, Ponce-Dawson S & Pearson JE (1998). Saltatory propagation of Ca^{2+} waves by Ca^{2+} sparks. *Biophys J* **75**, 595–600.

Kobayashi M & Musha T (1982). 1/f fluctuation of heartbeat period. *IEEE Trans Biomed Eng* **29**, 456–457.

Kucera JP, Heuschkel MO, Renaud P & Rohr S (2000). Power-law behavior of beat-rate variability in monolayer cultures of neonatal rat ventricular myocytes. *Circ Res* **86**, 1140–1145.

Lakatta EG, Maltsev VA & Vinogradova TM (2010). A coupled system of intracellular Ca^{2+} clocks and surface membrane voltage clocks controls the timekeeping mechanism of the heart's pacemaker. *Circ Res* **106**, 659–673.

Mahajan A, Shiferaw Y, Sato D, Baher A, Olcese R, Xie L-H, Yang M-J, Chen P-S, Restrepo JG, Karma A, Garfinkel A, Qu Z & Weiss JN (2008). A rabbit ventricular action potential model replicating cardiac dynamics at rapid heart rates. *Biophys J* **94**, 392–410.

Maltsev AV, Maltsev VA, Mikheev M, Maltseva LA, Sirenko SG, Lakatta EG & Stern MD (2011). Synchronization of stochastic Ca^{2+} release units creates a rhythmic Ca^{2+} clock in cardiac pacemaker cells. *Biophys J* **100**, 271–283.

Manly BFJ (1997). *Randomization, bootstrap and Monte Carlo methods in biology*. CRC Press, Boca Raton, FL, USA.

Marchant J, Callamaras N & Parker I (1999). Initiation of IP_3-mediated Ca^{2+} waves in *Xenopus* oocytes. *EMBO J* **18**, 5285–5299.

Marchant JS & Parker I (2001). Role of elementary Ca^{2+} puffs in generating repetitive Ca^{2+} oscillations. *EMBO J* **20**, 65–76.

Nivala M, de Lange E, Rovetti R & Qu Z (2012*a*). Computational modelling and numerical methods for spatiotemporal calcium cycling in ventricular myocytes. *Front Physiol* **3**, 114.

Nivala M, Ko CY, Nivala M, Weiss JN & Qu Z (2012*b*). Criticality in intracellular calcium signalling in cardiac myocytes. *Biophys J* **102**, 2433–2442.

Parker I, Choi J & Yao Y (1996). Elementary events of InsP3-induced Ca^{2+} liberation in *Xenopus* oocytes: hot spots, puffs and blips. *Cell Calcium* **20**, 105–121.

Ponard JG, Kondratyev AA & Kucera JP (2007). Mechanisms of intrinsic beating variability in cardiac cell cultures and model pacemaker networks. *Biophys J* **92**, 3734–3752.

Qu Z & Weiss JN (2005). Effects of Na^{+} and K^{+} channel blockade on vulnerability to and termination of fibrillation in simulated normal cardiac tissue. *Am J Physiol Heart Circ Physiol* **289**, H1692–H1701.

Ramay HR, Liu OZ & Sobie EA (2011). Recovery of cardiac calcium release is controlled by sarcoplasmic reticulum refilling and ryanodine receptor sensitivity. *Cardiovasc Res* **91**, 598–605.

Restrepo JG, Weiss JN & Karma A (2008). Calsequestrin-mediated mechanism for cellular calcium transient alternans. *Biophys J* **95**, 3767–3789.

Rooney TA, Sass EJ & Thomas AP (1990). Agonist-induced cytosolic calcium oscillations originate from a specific locus in single hepatocytes. *J Biol Chem* **265**, 10792–10796.

Rovetti R, Cui X, Garfinkel A, Weiss JN & Qu Z (2010). Spark-induced sparks as a mechanism of intracellular calcium alternans in cardiac myocytes. *Circ Res* **106**, 1582–1591.

Shuai JW & Jung P (2003). Optimal ion channel clustering for intracellular calcium signalling. *Proc Natl Acad Sci U S A* **100**, 506–510.

Simpson PB, Mehotra S, Lange GD & Russell JT (1997). High density distribution of endoplasmic reticulum proteins and mitochondria at specialized Ca^{2+} release sites in oligodendrocyte processes. *J Biol Chem* **272**, 22654–22661.

Skupin A & Falcke M (2009). From puffs to global Ca^{2+} signals: how molecular properties shape global signals. *Chaos* **19**, 037111.

Skupin A, Kettenmann H & Falcke M (2010). Calcium signals driven by single channel noise. *PLoS Comput Biol* **6**, e1000870.

Skupin A, Kettenmann H, Winkler U, Wartenberg M, Sauer H, Tovey SC, Taylor CW & Falcke M (2008). How does intracellular Ca^{2+} oscillate: by chance or by the clock? *Biophys J* **94**, 2404–2411.

Sobie EA, Dilly KW, dos Santos Cruz J, Lederer WJ & Jafri MS (2002). Termination of cardiac Ca^{2+} sparks: an investigative mathematical model of calcium-induced calcium release. *Biophys J* **83**, 59–78.

Sobie EA, Song LS & Lederer WJ (2006). Restitution of Ca^{2+} release and vulnerability to arrhythmias. *J Cardiovasc Electrophysiol* **17** (Suppl. 1), S64–S70.

Soeller C & Cannell MB (1999). Examination of the transverse tubular system in living cardiac rat myocytes by 2-photon microscopy and digital image–processing techniques. *Circ Res* **84**, 266–275.

Soeller C, Crossman D, Gilbert R & Cannell MB (2007). Analysis of ryanodine receptor clusters in rat and human cardiac myocytes. *Proc Natl Acad Sci U S A* **104**, 14958–14963.

Stanley HE (1999). Scaling, universality, and renormalization: Three pillars of modern critical phenomena. *Rev Mod Phys* **71**, S358–366.

Stern MD, Song LS, Cheng H, Sham JS, Yang HT, Boheler KR & Rios E (1999). Local control models of cardiac excitation-contraction coupling. A possible role for allosteric interactions between ryanodine receptors. *J Gen Physiol* **113**, 469–489.

ter Keurs HEDJ & Boyden PA (2007). Calcium and Arrhythmogenesis. *Physiol Rev* **87**, 457–506.

Thorn P, Lawrie AM, Smith PM, Gallacher DV & Petersen OH (1993). Local and global cytosolic Ca^{2+} oscillations in exocrine cells evoked by agonists and inositol trisphosphate. *Cell* **74**, 661–668.

Thurley K, Smith IF, Tovey SC, Taylor CW, Parker I & Falcke M (2011). Timescales of IP_3-evoked Ca^{2+} spikes emerge from Ca^{2+} puffs only at the cellular level. *Biophys J* **101**, 2638–2644.

Vinogradova TM, Brochet DX, Sirenko S, Li Y, Spurgeon H & Lakatta EG (2010). Sarcoplasmic reticulum Ca^{2+} pumping kinetics regulates timing of local Ca^{2+} releases and spontaneous beating rate of rabbit sinoatrial node pacemaker cells. *Circ Res* **107**, 767–775.

Vinogradova TM & Lakatta EG (2009). Regulation of basal and reserve cardiac pacemaker function by interactions of cAMP-mediated PKA-dependent Ca^{2+} cycling with surface membrane channels. *J Mol Cell Cardiol* **47**, 456–474.

Wagner J & Keizer J (1994). Effects of rapid buffers on Ca^{2+} diffusion and Ca^{2+} oscillations. *Biophys J* **67**, 447–456.

Wasserstrom JA, Shiferaw Y, Chen W, Ramakrishna S, Patel H, Kelly JE, O'Toole MJ, Pappas A, Chirayil N, Bassi N, Akintilo L, Wu M, Arora R & Aistrup GL (2010). Variability in timing of spontaneous calcium release in the intact rat heart is determined by the time course of sarcoplasmic reticulum calcium load. *Circ Res* **107**, 1117–1126.

Wier WG, ter Keurs HE, Marban E, Gao WD & Balke CW (1997). Ca^{2+} 'sparks' and waves in intact ventricular muscle resolved by confocal imaging. *Circ Res* **81**, 462–469.

Xie F, Qu Z, Garfinkel A & Weiss JN (2001*a*). Electrophysiological heterogeneity and stability of reentry in simulated cardiac tissue. *Am J Physiol Heart Circ Physiol* **280**, H535–H545.

Xie F, Qu Z, Weiss JN & Garfinkel A (2001*b*). Coexistence of multiple spiral waves with independent frequencies in a heterogeneous excitable medium. *Phys Rev E Stat Nonlin Soft Matter Phys* **63**, 031905.

Xie Y, Sato D, Garfinkel A, Qu Z & Weiss JN (2010). So little source, so much sink: requirements for afterdepolarizations to propagate in tissue. *Biophys J* **99**, 1408–1415.

Zeng WZ, Glass L & Shrier A (1991). Evolution of rhythms during periodic stimulation of embryonic chick heart cell aggregates. *Circ Res* **69**, 1022–1033.

Additional information

Competing interests

None.

Author contributions

All authors contributed to the research design, data analysis, manuscript drafting and revision; M.N. and M.N. carried out the computer programming and simulations; C.K. did the myocyte experiments and statistical analysis; M.N. and Z.Q. developed the theory; Z.Q. conceived the overall research. All authors have read and approved the final version of the manuscript.

Funding

This work was supported by National Institute of Health grant P01 HL078931; American Heart Association, Western States Affiliate, Postdoctoral Fellowship Award 10POST3210024 (M.N.), Predoctoral Fellowship Award 10PRE3030052 (C.K.); the Laubisch and Kawata Endowments; and the UCLA Cardiovascular Development Fund (M.N.).

Acknowledgements

We thank Alan Garfinkel, Hrayr Karagueuzian, Riccardo Olcese, and the members of the UCLA arrhythmia group for helpful comments, Rahil D. Patel for cell preparation, and Guillaume Calmettes for help in statistical analysis.